

Bayesian pathway analysis over brain network mediators for survival data

Xinyuan Tian¹, Fan Li^{1,2,3}, Li Shen^{1,4}, Denise Esserman^{1,2}, Yize Zhao^{1,2,*}

¹Department of Biostatistics, Yale School of Public Health, New Haven, CT 06511, United States, ²Yale Center for Analytical Sciences, Yale School of Public Health, New Haven, CT 06511, United States, ³Center for Methods in Implementation and Prevention Science, Yale School of Public Health, New Haven, CT 06511, United States, ⁴Department of Biostatistics, Epidemiology and Informatics, University of Pennsylvania, Philadelphia, PA 19104, United States

*Corresponding author: Yize Zhao, Department of Biostatistics, Yale School of Public Health, Yale University, 300 Gerge St. New Haven, CT 06511, USA (yize.zhao@yale.edu).

ABSTRACT

Technological advancements in noninvasive imaging facilitate the construction of whole brain interconnected networks, known as brain connectivity. Existing approaches to analyze brain connectivity frequently disaggregate the entire network into a vector of unique edges or summary measures, leading to a substantial loss of information. Motivated by the need to explore the effect mechanism among genetic exposure, brain connectivity, and time to disease onset with maximum information extraction, we propose a Bayesian approach to model the effect pathway between each of these components while quantifying the mediating role of brain networks. To accommodate the biological architectures of brain connectivity constructed along white matter fiber tracts, we develop a structural model which includes a symmetric matrix-variate accelerated failure time model for disease onset and a symmetric matrix response regression for the network-variate mediator. We further impose within-graph sparsity and between-graph shrinkage to identify informative network configurations and eliminate the interference of noisy components. Simulations are carried out to confirm the advantages of our proposed method over existing alternatives. By applying the proposed method to the landmark Alzheimer's Disease Neuroimaging Initiative study, we obtain neurobiologically plausible insights that may inform future intervention strategies.

KEYWORDS: accelerated failure time model; brain connectivity; imaging genetics; mediation analysis; natural indirect effect; shrinkage and regularization.

1 INTRODUCTION

The field of network neuroscience acknowledges that a brain nervous system is defined by interconnections of its neuronal units. Through advances in noninvasive imaging techniques, one could establish a cartography of these neuronal interconnections known as brain connectivity. Compared with regional neuroimaging measurements that characterize brain structure or function at separate locations, whole-brain connectivity provides unique descriptions of neuronal patterns, and is expected to align with different types of brain activities.

Although successes have been achieved in relating connectivity with human behavior, most of these studies were based on healthy individuals. It is likely that important disease metrics, such as time to disease onset, are associated with altered brain patterns and their relationship may further be shaped by potential exposure factors. The methods proposed in this article are motivated by Alzheimer's disease (AD), a neurodegenerative disease where brain atrophy leads to cognitive decline. Besides neurological changes, the risk and progression of AD are strongly influenced by genetics. The most prominent genetic risk factor identified is the $\epsilon 4$ allele of the APOE gene (APOE4), which is known to substantially increase the disease risk and lower

the onset age of AD. Recent advances in neuroimaging genetics have started to substitute disease phenotypes with imaging endophenotypes to explore the potentially associated genetic variants (Hashimoto et al., 2015). However, the pathological mechanism among genetic factors, neuroimaging traits, and disease outcomes is yet to be fully elucidated.

To uncover the effect mechanism among the genetic exposure, brain structural connectivity defined by white matter fiber tracts, and time to AD onset, we propose a Bayesian mediation framework with a time-to-event outcome and a network-variate mediator. Mediation analysis has been developed to understand the mechanisms relating to how one phenomenon exerts its influence on another, via an intermediate variable. By partitioning the overall effect on a dependent variable into a direct effect coming from an independent variable and an indirect effect passing through a mediator, one is able to dissect the effect pathways functioning among different components. The initial implementations of mediation analysis focus on a single mediator with a continuous outcome (Imai and Yamamoto, 2013), with extensions to accommodate multivariate or high-dimensional mediators (Derkach et al., 2019; Song et al., 2020) and other types of outcomes, including binary (Wang et al., 2013) and

time-to-event (Huang and Yang, 2017) outcomes. Most of the studies applying these methods to neuroimaging data consider mediating traits in a scalar or vector form summarized by regional imaging measurements (Lindquist, 2012; Zhao and Luo, 2019; Chén et al., 2018; Zhao et al., 2021). More recently, Zhao et al. (2022) initiated an early effort to handle brain functional connectivity as a mediator. However, they considered a continuous outcome and assumed a stochastic block structure for the mediating networks, which is not applicable for our motivating example as it involves brain structural connectivity with distinct network architectures and a time-to-event outcome subject to right censoring.

To properly model this complicated neurobiological mechanism, it is essential to characterize the unique topological form of structural connectivity with biological interpretability. Current analyses on structural connectivity primarily represent the whole network as a vector of unique edges or summary measures (Ballester-Plané et al., 2017; Chen et al., 2022), resulting in a loss of topological information. Wang et al. (2021) summarize the connectivity via a number of small clique subgraphs, which aligns with the biological architecture of white matter fiber traits. Taking this idea further, we propose that structural connectivity mediates the relationship through a set of signaling subgraphs that are influenced by the genotype and affect the disease onset outcome. To uncover the effect mechanism, we propose a structural modeling framework including a symmetric matrix-variate accelerated failure time (AFT) model for the effect pathway from brain connectivity to the outcome, and a symmetric matrix response regression for the effect pathway from the genetic exposure to brain connectivity. Under a Bayesian paradigm, we impose within-graph sparsity to select important network configurations, along with between-graph shrinkage to eliminate undesirable interference from noisy elements. To our best knowledge, each of the above novel modeling components itself has not yet been considered in previous brain imaging studies.

The remainder of the article is organized as follows. In Section 2, we introduce a new network-variate mediation framework with symmetric and hollow structural constraints. In Section 3, we discuss the prior specifications and develop the posterior sampling procedures for statistical inference. We conduct simulation studies to evaluate the model performance in Section 4, and implement our method to data extracted from Alzheimer's Disease Neuroimaging Initiative (ADNI) study in Section 5. Section 6 concludes.

2 METHODS

2.1 Model formulation

We start with a general model formulation. For subject i ($i = 1, \dots, N$), let T_i denote the time to disease onset, and C_i the right censoring time. The observed follow-up time can be represented as $\tilde{T}_i = \min\{T_i, C_i\}$, and we define a censoring indicator $\delta_i = 1$ if an event is observed and 0 if censored. Let z_i represent the binary exposure, corresponding to the APOE4 positivity (APOE4+) in our application characterizing the presence of at least one $\epsilon 4$ allele. Meanwhile, $\mathbf{x}_i \in \mathbb{R}^{Q \times 1}$ represents a set

of covariates to be adjusted for, including an intercept. We assume the brain structural connectivity can be summarized by a graph $\mathcal{G}_i = (\mathcal{R}, \mathcal{E}_i)$ with a common set of nodes \mathcal{R} and subject-specific edges \mathcal{E}_i . Given the graphs are defined under the same brain atlas, the shared set of nodes is defined by a total of R brain regions of interest (ROIs) within which we extract data from voxels. Subsequently, we represent \mathcal{G}_i by a symmetric connectivity matrix $\mathbf{A}_i \in \mathbb{R}^{R \times R}$; its (w, l) th entry a_{iwl} is a continuous variable characterizing the white matter fiber density value between ROIs w and l , $0 < w \neq l \leq R$. By construction, \mathbf{A}_i is a hollow matrix with $a_{iwl} = 0$, if $0 < w = l \leq R$.

Our goal is to characterize the potential pathways among the time-to-event outcome, APOE4 genotype, and brain structural connectivity. Simultaneously, we aim to identify brain subgraph configurations that function along each effect path where the neural system is involved. As stated previously, it is important to maintain the topological architectures of brain connectivity. On the one hand, different from social networks, each connectivity matrix \mathbf{A}_i is symmetric and with a hollow structure corresponding to the bidirectional structural connectivity with no self-connections. On the other hand, structural connectivity could operate under distinct topological structures when linked with genetics and disease profiles. With those considerations, we propose the following structural models

$$\log(T_i) = \mathbf{x}_i^T \boldsymbol{\beta}_x + \left\langle \sum_{j=1}^J \omega_j \boldsymbol{\beta}_j \boldsymbol{\beta}_j^T, \mathbf{A}_i \right\rangle_F + \beta_z z_i + \epsilon_i; \quad (1)$$

$$\mathbf{A}_i = \mathbf{G}_i - \text{Dg}[\mathbf{G}_i] + \mathbf{E}_i;$$

$$\mathbf{G}_i = \mathcal{M} \times_3 \mathbf{x}_i^T + \sum_{h=1}^H \eta_h \boldsymbol{\alpha}_h \boldsymbol{\alpha}_h^T z_i. \quad (2)$$

Model (1) captures the effects on the time-to-event outcome through an AFT model with $\boldsymbol{\beta}_x \in \mathbb{R}^{Q \times 1}$ and β_z representing the effects of covariates and exposure on the logarithmic survival time, respectively. We assume $\epsilon_i \sim N(0, \sigma_0^2)$ in our application without loss of generality, as other parametric distributions such as log-normal or extreme value distributions could also be adopted with minor modifications. For the mediator model, given it is common to assume a low-rank structure for brain connectivity data (Zhao et al., 2023), we adopt a symmetric tensor rank- J Tucker decomposition (Kolda and Bader, 2009) which is synonymous with an eigenvalue decomposition for a symmetric matrix by representing the mediator-specific coefficient matrix via $\sum_{j=1}^J \omega_j \boldsymbol{\beta}_j \boldsymbol{\beta}_j^T$; the connectivity matrix then associates with the outcome by a Frobenius inner product $\langle \cdot, \cdot \rangle_F$. From a neurobiological perspective, such a representation allows us to capture the impact from structural connectivity through a combination of J network configurations, corresponding to the aforementioned subgraphs. Each subgraph j is represented through a matrix $\omega_j \boldsymbol{\beta}_j \boldsymbol{\beta}_j^T$ with coefficients $\boldsymbol{\beta}_j \in \mathbb{R}^{R \times 1}$ describing the within subgraph effect of each node, and ω_j capturing the impact between subgraphs. Given that different brain network configurations are employed under distinct neuronal processes, it is assumed each $\boldsymbol{\beta}_j$ is sparse to induce a specific clique structure

contributing to the effect pathway on the outcome. Importantly, introducing sparsity with a Tucker decomposition will reduce the burden of estimating parameters over a high-dimensional feature space. The technical details on sparsity will be discussed in Section 3.1.

Along with model (1), model (2), which consists of 2 sub-models, captures the impact from the exposure to the connectivity mediator. With \mathbf{A}_i on the left-hand side of the equation, we essentially have a network response regression, where the network is constrained by a symmetric and hollow structure. To align with the 0 diagonal elements of \mathbf{A}_i , we first denote the matrix-variate effect from the covariates and exposure as \mathbf{G}_i . Within \mathbf{G}_i , $\mathcal{M} \in \mathbb{R}^{R \times R \times Q}$ is the coefficient tensor adjusting for the effects from the covariates, and we expect \mathcal{M} to be semi-symmetric under frontal slices given each $\mathcal{M}_{\dots,q}$ is symmetric. Similar to the operation in model (1), we employ a symmetric rank- H Tucker decomposition such that the impact from exposure to connectivity functions is through H subgraphs, and that the structural configuration of subgraph h is captured by $\alpha_h \in \mathbb{R}^{R \times 1}$ with weight η_h . Since the model formulation for \mathbf{G}_i only guarantees a symmetric structure, to ultimately link \mathbf{G}_i with the hollow matrix \mathbf{A}_i , we will remove the diagonal elements from \mathbf{G}_i denoted by $\text{Dg}[\mathbf{G}_i]$ while keeping the off-diagonal elements unaffected. For the residual error matrix \mathbf{E}_i which is also specified to be symmetric and hollow, we represent a collection of its upper-diagonal elements as a vector $\mathbf{e}_i \in \mathbb{R}^{R(R-1)/2 \times 1}$, and assume $\mathbf{e}_i \sim \mathbf{N}(\mathbf{0}, \mathbf{\Xi})$. In our numerical studies, we consider 3 implementations for covariance matrix $\mathbf{\Xi}$ by assuming (1) $\mathbf{\Xi}$ is a general covariance matrix to accommodate arbitrary correlations among connections, (2) a Bayesian factor model (Zhu et al., 2014) that introduces a low-rank representation for $\mathbf{\Xi}$, and (3) $\mathbf{\Xi} = \sigma_1^2 \mathbf{I}$ to reduce the computational complexity. Finally, as demonstrated previously in Bayesian tensor regression models, although the margins for β_j and α_h may not be identifiable, the coefficient matrices (Guhaniyogi et al., 2017) and subgraph configurations under our model structure (Tian et al., 2024) are uniquely determined.

It is worth emphasizing that in practice, different types of brain connectivity preserve distinct biological architectures. For example, brain functional connectivity tends to present a modular structure to calibrate different functional systems. We study structural connectivity here by modeling the subgraph structures along effect pathways, consistent with the densely connected white matter fiber tracks within certain nodes for efficient neural support (Bassett and Sporns, 2017). Our approach is in sharp contrast to Zhao et al. (2022) where functional connectivity represented by modular structure serves as the mediator for a continuous outcome.

2.2 Effect pathways

To quantify the effect pathways among the survival outcome, exposure, and network-variate mediator, we introduce counterfactual representations to define the effect measures under the structural modeling framework. Let $\mathbf{A}(Z)$ be the value of the connectivity mediator under exposure Z with $Z = z$ or $Z = z^*$ denoting the 2 possible states. Let $T(Z, \mathbf{A}(Z))$ be the counterfactual survival time under Z and mediator $\mathbf{A}(Z)$. Given the co-

variates $\mathbf{X} = \mathbf{x}$, we define the natural indirect effect (NIE), natural direct effect (NDE), and total effect (TE) as

$$\begin{aligned} \text{NIE} &= \mathbb{E}[\log\{T(z, \mathbf{A}(z)) \mid \mathbf{X} = \mathbf{x}\}] \\ &\quad - \mathbb{E}[\log\{T(z, \mathbf{A}(z^*)) \mid \mathbf{X} = \mathbf{x}\}]; \\ \text{NDE} &= \mathbb{E}[\log\{T(z, \mathbf{A}(z^*)) \mid \mathbf{X} = \mathbf{x}\}] \\ &\quad - \mathbb{E}[\log\{T(z^*, \mathbf{A}(z^*)) \mid \mathbf{X} = \mathbf{x}\}]; \\ \text{TE} &= \text{NIE} + \text{NDE} = \mathbb{E}[\log\{T(z, \mathbf{A}(z)) \mid \mathbf{X} = \mathbf{x}\}] \\ &\quad - \mathbb{E}[\log\{T(z^*, \mathbf{A}(z^*)) \mid \mathbf{X} = \mathbf{x}\}]. \end{aligned} \tag{3}$$

Following common practice for time-to-event outcomes (Van der Weele, 2011), model (3) defines each effect component on the log-survival time scale aligning with the AFT model. In our specific application, NIE quantifies the expected change in log-survival time when the connectivity mediator changes from $\mathbf{A}(z^*)$ to $\mathbf{A}(z)$ with fixed genetic exposure; NDE characterizes the expected change in log-survival time by altering the genetic exposure when brain connectivity is fixed; and TE is the sum of NIE and NDE, and hence captures the overall change in log-survival time under different states of genetic exposure. We have the following proposition for each effect component.

Proposition 1 Under the proposed structural model represented by (1) and (2) and definitions of the different effect components in (3), it can be shown that

$$\begin{aligned} \text{NIE} &= (z - z^*) \sum_{j=1}^J \sum_{h=1}^H \\ &\quad \times \left\langle \omega_j \beta_j \beta_j^T, (\eta_h \alpha_h \alpha_h^T - \eta_h \text{Dg}[\alpha_h \alpha_h^T]) \right\rangle_F, \\ \text{NDE} &= \beta_z (z - z^*) \\ \text{TE} &= (z - z^*) \sum_{j=1}^J \sum_{h=1}^H \\ &\quad \times \left\langle \omega_j \beta_j \beta_j^T, (\eta_h \alpha_h \alpha_h^T - \eta_h \text{Dg}[\alpha_h \alpha_h^T]) \right\rangle_F \\ &\quad + \beta_z (z - z^*). \end{aligned} \tag{4}$$

The detailed derivations for the above proposition are provided in [Web Appendix A.2](#).

Compared with the effect measures under an existing mediation analysis with a scalar or vector mediator, the above proposition reveals that the structural connectivity mediator contributes to the TE and NIE by combining subgraphs identified along the exposure to mediator effect pathway, and those identified along the mediator to outcome effect pathway. Moreover, we conclude from (4) that there are subgraphs that absorb impact from the exposure without changing the outcome; and subgraphs that alter the outcome intrinsically without interacting with the exposure. To further elaborate, Figure 1 illustrates this observation using an illustrative example of 2 informative subgraphs from the exposure to mediator pathway, and 2 informative subgraphs from the mediator to survival outcome pathway. Eventually, the potential mediators are the overlapping configurations that im-

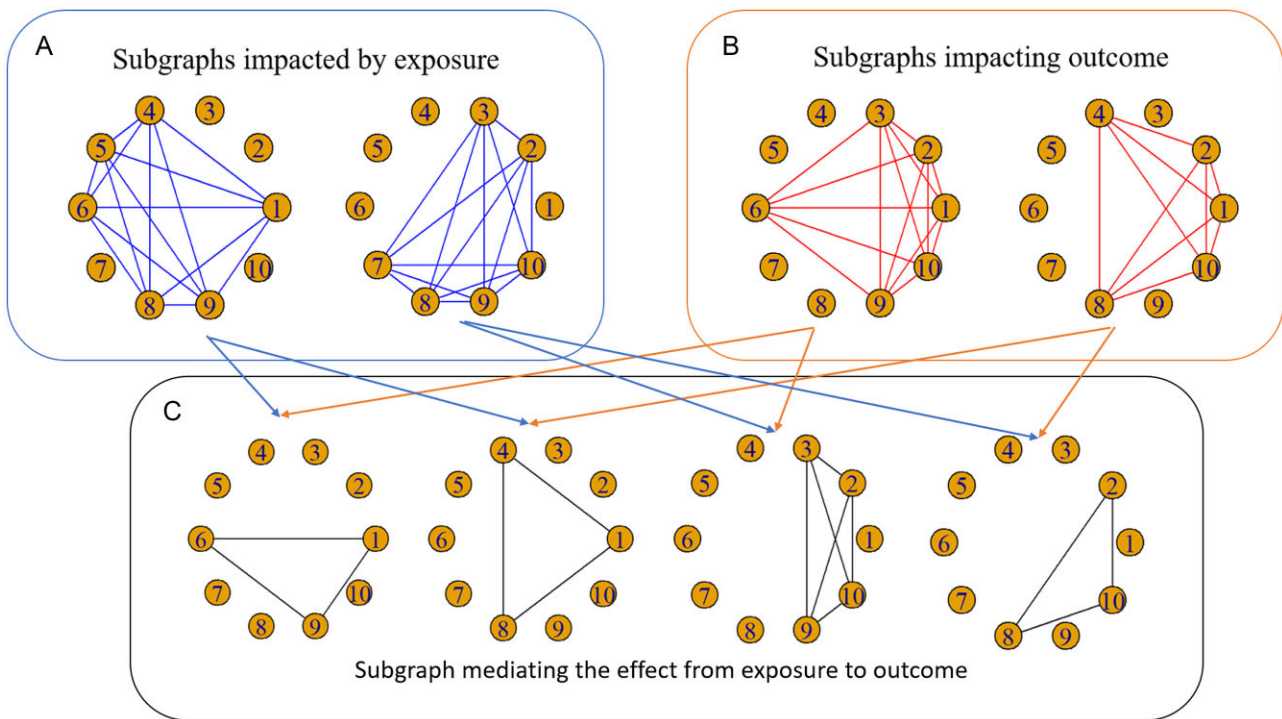


FIGURE 1 As an illustration, the upper panels show (A) 2 informative subgraphs from the exposure to mediator effect pathway, and (B) 2 informative subgraphs from the mediator to survival outcome effect pathway. The bottom panel provides (C) the active mediating components contributing to the natural indirect effect (NIE), which consist of the overlapping network configuration.

both pathways as shown in the lower panel of Figure 1. In [Web Appendix A.2](#), we also discuss an alternative definition for effects using log-expected survival times, and show that the ultimate formulations for each effect metric are identical under different definitions. It is also worth noting that within the causal mediation framework, several structural assumptions (Imai et al., 2010) are required for a causal interpretation under a structural regression framework. However, these assumptions are often unverifiable from the observed data, and it is possible that not all confounders are measured in a single study. In our brain imaging application, due to the potential for unmeasured confounding, we employ our mediation method as an exploratory tool for associational analysis to generate useful hypotheses, rather than a conclusive tool for causal inference. Despite our focus on associational analysis, we provide the identification assumptions for causal interpretation in [Web Appendix A.1](#).

3 BAYESIAN INFERENCE

3.1 Prior specification

We propose a Bayesian algorithm to estimate the model parameters. Compared with mediation methods under a frequentist paradigm, Bayesian modeling is particularly attractive due to its ability in automatically capturing the uncertainty for all effect estimates with complex modeling (Schoot et al., 2013). As mentioned previously, extracting informative brain subgraphs for each path captured by $\{\beta_j, \omega_j\}_{j=1}^J$ and $\{\alpha_h, \eta_h\}_{h=1}^H$ is as important as estimating the NIE, NDE, and TE for uncovering

the effect pathways. Denoting $\beta_j = (\beta_{j1}, \dots, \beta_{jR})^T$ and $\alpha_h = (\alpha_{h1}, \dots, \alpha_{hR})^T$, we assign point mass mixture priors for each element of β_j and α_h to impose sparsity as

$$\begin{aligned} \beta_{jr} &\sim (1 - \gamma_{jr})N(0, \nu_0) + \gamma_{jr}N(0, \nu_1); \\ \alpha_{hr} &\sim (1 - \tau_{hr})N(0, \nu_0) + \tau_{hr}N(0, \nu_2), \end{aligned} \quad (5)$$

with $j = 1, \dots, J$; $h = 1, \dots, H$; $r = 1, \dots, R$. Here, ν_0 represents a very small variance component, ν_1 and ν_2 are variance components with a large value, and γ_{jr} and τ_{hr} are the latent selection indicators introduced to identify nonzero elements within the 2 sets of network-variant coefficients. Specifically, in the case of $\gamma_{jr} = 1$, we have $\beta_{jr} \neq 0$, indicating that the connections linked with node r represent an informative subgraph impacting the time to disease onset. Similarly, when $\tau_{hr} = 1$, we have $\alpha_{hr} \neq 0$ indicating that connections linked with node r represent an informative subgraph influenced by the genetic exposure.

To specify priors for $\boldsymbol{\gamma} = \{\gamma_{1r}, \dots, \gamma_{Jr}\}_{r=1}^R$ and $\boldsymbol{\tau} = \{\tau_{1r}, \dots, \tau_{Hr}\}_{r=1}^R$, one can either impose a noninformative Bernoulli distribution for each of the elements, or resort to a more informative prior by incorporating knowledge of biological structure. Such structural information includes brain regions located symmetrically between right and left brain hemispheres, or networks coming from nodes that are connected at the population level. To first summarize the information, one could consider an undirected knowledge graph \mathcal{G}_0 by including an edge if 2 nodes are symmetric on hemispheres or connected populationally, and then encourage smoothness on selection over \mathcal{G}_0 using a Markov random field (MRF) prior (Sun et al.,

2018)

$$p(\boldsymbol{\gamma}, \boldsymbol{\tau}) \propto \exp \left\{ \mu \sum_r \left(\sum_{j=1}^J \gamma_{jr} + \sum_{h=1}^H \tau_{hr} \right) + \nu \sum_{r \sim r'} \left(\sum_{j=1}^J \gamma_{jr} \gamma_{jr'} + \sum_{h=1}^H \tau_{hr} \tau_{hr'} \right) \right\} \quad (6)$$

with $r \sim r'$ indicating a connection at \mathcal{G}_0 . In model (6), μ controls the number of nodes selected in a subgraph, and η impacts the smoothness reflected by the degree of confidence to include both nodes in the informative subgraphs if they are connected at a prior level. When both $\mu = \nu = 0$, model (6) degenerates to noninformative Bernoulli distributions without incorporating prior structural information. In addition, the weights $\{\omega_j\}_{j=1}^J$ and $\{\eta_h\}_{h=1}^H$ characterize graph-level effects for the J subgraphs impacting the outcome and H subgraphs influenced by the exposure. To distinguish the role each subgraph plays in the effect mechanism, and more importantly to shrink the effects associated with subgraphs that link loosely with both outcome and exposure, we assign Laplace priors (Park and Casella, 2008) as

$$\omega_j \sim \mathcal{L}(\lambda_\omega); \quad \eta_h \sim \mathcal{L}(\lambda_\eta); \\ j = 1, \dots, J; \quad h = 1, \dots, H, \quad (7)$$

with shrinkage parameters λ_ω and λ_η . Since J and H are unknown in practice, the Laplace priors, along with the shrinkage parameters, allow the model to eliminate noise graph for more efficient inference about the effect pathways.

For the remaining parameters, most of them will be assigned canonical priors chosen by analytical convenience including $\beta_x \sim N(\mathbf{0}, \mathbf{I}\sigma_x^2)$ and $\beta_z \sim N(0, \sigma_z^2)$. We further assume the coefficient tensor \mathcal{M} , which associates the covariates with the connectivity mediator, follows a symmetric rank- K tensor decomposition as $\mathcal{M} = \sum_{k \in [K]} \mathbf{a}_{1k} \circ \mathbf{a}_{1k} \circ \mathbf{a}_{2k}$ with $\mathbf{a}_{1k} \in \mathbb{R}^{R \times 1}$, $\mathbf{a}_{2k} \in \mathbb{R}^{Q \times 1}$ to downsize the number of parameters and $\mathbf{a}_{1k} \sim N(\mathbf{0}, \mathbf{I}\sigma_a^2)$ and $\mathbf{a}_{2k} \sim N(\mathbf{0}, \mathbf{I}\sigma_a^2)$ for $k = 1, \dots, K$. For the covariance matrix Ξ , we consider 3 different implementations and assign corresponding priors accordingly. When assuming an unstructured covariance, we assign an Inverse Wishart prior $IW(\mathbf{I}, \frac{R(R-1)}{2})$ to Ξ . For working independence, where $\Xi = \sigma_a^2 \mathbf{I}$, we specify noninformative inverse gamma (IG) priors with shape and scale parameters both set to 0.01 for σ_a^2 . Additionally, detailed prior specifications for Ξ using the Bayesian factor model are provided in Web Appendix B. We then assign $IG(0.01, 0.01)$ for variances σ_z^2 , σ_0^2 , and set a large value (ie, 10) for the remaining variance hyper-parameters σ_a^2 , σ_x^2 .

Finally, there are a few tuning parameters required to be pre-specified, including H and J , decomposition rank K , and sparsity and smoothness parameters μ and ν when the MRF prior is used. Given \mathcal{M} is a nuisance parameter, we directly specify K to be a finite number. In our application, we set $K = 3$ to capture sufficient information in \mathcal{M} . For the rest of the tuning parameters, we consider a grid of values, and implement our model under all parameter combinations. Then, we empirically choose the optimal fit using the Bayesian information criterion (BIC). We name our model **Bayesian SuGraph-based Mediation**

(BSGM) analysis with a diagonal Ξ , and refer to the more complex version with an Bayesian factor model for Ξ as **Bayesian SuGraph-based Mediation with factor model** (BSGM_{fm}) analysis. We also include a version with unstructured Ξ as **Bayesian SuGraph-based Mediation with correlation** (BSGM_{cor}) analysis. We present a schematic illustration of our analytical framework in Web Figure 1.

3.2 Posterior inference

Given the observed data $\mathcal{O} = \{\tilde{T}_i, \mathbf{A}_i, \mathbf{x}_i, z_i, \delta_i; i = 1, \dots, N\}$, the unknown parameters $\Theta = [\beta_x, \beta_z, \{\alpha_h, \eta_h\}_{h=1}^H, \{\beta_j, \omega_j\}_{j=1}^J, \boldsymbol{\tau}, \boldsymbol{\gamma}, \{\mathbf{a}_{1k}, \mathbf{a}_{2k}\}_{k=1}^K, \sigma_z^2, \sigma_0^2, \sigma_1^2, \Xi]$ follow the joint posterior distribution:

$$f(\Theta | \mathcal{O}) \prod_i \{\delta_i f(\tilde{T}_i | \Theta) + (1 - \delta_i) S(\tilde{T}_i | \Theta)\} \prod_i f(\mathbf{A}_i | \Theta) \\ \times \prod_h \prod_j \{f(\eta_h) f(\omega_j) f(\alpha_h | \boldsymbol{\tau}_h) f(\beta_j | \boldsymbol{\gamma}_j) f(\boldsymbol{\gamma}_j) f(\boldsymbol{\tau}_h)\} \\ \times f(\beta_x) f(\beta_z) f(\Xi) f(\sigma_1^2) f(\sigma_0^2) f(\sigma_z^2) \\ \times \prod_k \{f(\mathbf{a}_{1k}) f(\mathbf{a}_{2k})\},$$

where $f(\tilde{T}_i | \Theta)$ and $S(\tilde{T}_i | \Theta)$ are the density and survival functions for the time to disease onset implied from our structural AFT model, respectively. Under our current model assumptions, with no shared parameters between model (1) and (2), the joint posterior distribution of the 2 models can be expressed as the product of the posterior distributions of each individual model. To draw samples from the posterior distribution for inference, we develop a tractable Markov chain Monte Carlo (MCMC) algorithm through Gibbs samplers. In particular, we address censored values using data augmentation, where the unobserved survival times are imputed in every Gibbs iteration. A brief overview of the sampling steps for BSGM, BSGM_{fm}, and BSGM_{cor}, along with the detailed sampling procedure, can be found in Web Appendix B.

After obtaining the posterior samples from the above MCMC algorithm, based on the marginal posterior probability for the elements in $\boldsymbol{\gamma}$ and $\boldsymbol{\tau}$, and the posterior mean for each $\{\omega_j\}_{j=1}^J$ and $\{\eta_h\}_{h=1}^H$, we are able to identify the informative brain subgraph configurations along each effect pathway. The informative connections within the subgraph are then determined based on the posterior probability of $\boldsymbol{\gamma}$ and $\boldsymbol{\tau}$ using a cutoff value of 0.5 in the spirit of the median probability model (Barbieri and Berger, 2004). Subsequently, the posterior mean estimates for the NIE, NDE, and TE and the corresponding 95% credible intervals can be obtained directly according to the identification formulas given in (4).

4 SIMULATION STUDY

We carry out simulation studies to evaluate the performance of the proposed mediation methods. To mimic the data dimension in our application, we consider sample sizes of $N = 100$ and 500 with each subject's brain connectivity $R = 100$. For the exposure, we generate $z_i \sim \text{Bern}(0.5)$ and consider 3 covari-

ates in addition to the intercept with the first 2 covariates generated from $N(0, 1)$ and the last generated from $\text{Bern}(0.65)$. We set $\beta_z = 1.4$, $\beta_x = (1.4, 0.8, 0.5)^T$ and generate the coefficient tensor \mathcal{M} based on a rank-3 symmetric decomposition with $\mathbf{a}_{1k} \sim N(0, 0.4)$, $\mathbf{a}_{2k} \sim N(0, 0.4)$ for $k = 1, 2, 3$. For the informative network configurations linked with the exposure and outcome, we consider 2 clique subgraphs with each of them containing 8 nodes for the effect pathway to the outcome and another separate subgraph containing 10 nodes for the pathway from the exposure. For the effect coefficients associated with each subgraph which are represented by a symmetric matrix, instead of generating them through the vector outer product as assumed by our model, we simulate them from a Wishart distribution using a Toeplitz matrix as the scale matrix. For the random errors of the network mediator, we consider 2 scenarios—one where the potentially correlated errors (Cor) are generated from a Wishart distribution with a randomly simulated Toeplitz scale matrix, and one where the independent errors (Ind) are drawn from a Normal density with $\sigma_1^2 = 0.8$. Such different data generating processes could facilitate the comparison between BSGM and its variations—BSGM_{cor}, BSGM_{fm}—under different underlying correlation structures of the network mediator. To assess the model fit under different censoring schemes, we generate the censoring time C_i under 2 scenarios: (1) independent censoring with $C_i \sim \mathcal{E}(0.04)$ where $\mathcal{E}(\cdot)$ denotes an Exponential distribution; and (2) covariate-dependent censoring with $C_i \sim \mathcal{E}(\phi^T \mathbf{x}_i)$, where $\phi = (0.03, 0.02, 0.04)^T$. After obtaining \tilde{T}_i , we compare with C_i and directly determine the censoring indicator δ_i . The censoring rates for scenarios A and B are 35% and 30%, respectively. For each setting, we calculate the true effect measures (NIE, NDE, and TE) according to the identification formulas (4) as our true estimands. In total, we consider 8 simulated settings, and we generate 250 Monte Carlo datasets for each setting for evaluation.

To implement the proposed BSGM along its 2 variations BSGM_{fm} and BSGM_{cor}, we adopt noninformative Bernoulli priors for $\boldsymbol{\gamma}$ and $\boldsymbol{\tau}$. The MCMC algorithm runs under random initials for 5000 iterations with 1000 burn-in. The posterior convergence is monitored using both trace plots and the Gelman–Rubin method (Gelman et al., 1992). The optimal value of J and H is determined by BIC under a grid search from 5 to 12. The computational time to complete the full posterior inference for BSGM, BSGM_{fm} and BSGM_{cor} is approximately 8 h, 13 h, and 17 h, respectively (Yale High-Performance Computing, one CPU core, 3GB RAM). Given none of the existing methods can incorporate a network mediator with a survival outcome, we first consider existing univariate or multivariate mediator methods for comparison. Specifically, we vectorize the upper diagonal elements of each \mathbf{A}_i and include each connection as a mediator for univariate-mediator mediation analyses under the R package `mediation` (UMA), as well as all of them jointly for multivariate-mediator mediating analysis implemented by the R package `mma` (MMA). In addition, we consider the Bayesian network mediation model (BNMM) (Zhao et al., 2022), which is to our best knowledge, the only method that can handle a network mediator. Given the BNMM is designed for continuous outcomes, we adapt its model formulation to accommodate survival outcomes (detailed in Web Appendix B.1). Finally,

to evaluate the performance of each method, we consider the mean or posterior mean (*Mean*), percentage bias (*Bias*), and frequentist coverage rate (*Coverage*) by the 95% confidence interval (UMA, MMA) or the 95% credible interval (BSGM, BSGM_{fm}, BSGM_{cor}, BNMM) for estimating NIE, NDE, and TE, as well as the *Sensitivity* and *Specificity* for selecting the active mediators. To maintain consistency, the identified mediating subgraphs or edges are always mapped back to the same input connectivity matrix before compared with the ground truth. The simulation results are summarized in Table 1.

Based on the simulation results, we observe that our proposed BSGM, BSGM_{fm}, and BSGM_{cor} outperform all competing methods in uncovering effect mechanisms across all settings. Our methods achieve a small percentage bias, close to 90%–95% coverage for all the effect components (NIE, NDE and TE), and close to 100% sensitivity and specificity for identifying the active mediating subgraphs. These results indicate the strong capacity of our methods to uncover each effect pathway and its related brain network signals. For the competing methods, UMA and MMA have unsatisfactory performance, presenting much larger estimation bias and more conservative identification of mediators. This is expected given the network configurations along each effect pathway are completely eliminated in these methods. The BNMM, though considering a network mediator as a whole unit before decomposing it via stochastic block structures, fails to reflect the underlying subgraph configurations, leading to compromised accuracy in estimation and identification under our data generating mechanisms. As for the comparison among BSGM, BSGM_{fm}, and BSGM_{cor}, the performance of BSGM and its variations is highly consistent regardless of the true correlation structure for the network mediator. Notably, in settings with a smaller sample size, BSGM even slightly outperforms BSGM_{fm} and BSGM_{cor} when the network mediator has a non-independent correlation structure, possibly due to the reduced number of unknown parameters required to be estimated under a parsimonious specification.

Lastly, we also perform additional simulations in the presence of noise subgraphs included in the data generation and consider different sample sizes and censoring schemes. The detailed results of this set of simulations are presented in Web Appendix C. The findings there are in line with the conclusions from our primary simulations.

5 APPLICATION TO THE ADNI STUDY

We apply our method to the data extracted from the ADNI database (adni.loni.usc.edu). The ADNI including ADNI1, ADNI GO/2, and ADNI3 was launched in 2003 by the NIA, NIBIB, FDA, private pharmaceutical companies, and nonprofit organizations, as a public–private partnership. The goal of the study was to test whether serial magnetic resonance imaging (MRI), positron emission tomography, other biological markers, and clinical and neuropsychological assessment can be combined to measure the progression of mild cognitive impairment and early AD. In our current application, we are interested in exploring the effect pathways among APOE+, brain structural connectivity and time to AD onset right-censored by death or loss to follow-up. We focus on the 119 ADNI2 participants who

TABLE 1 Simulation results under different sample sizes, residual error distributions (Dep, dependent; Ind, independent), censoring mechanisms (A) independent censoring and (B) covariate-dependent censoring.

Residual Error	Scenario	N = 100										N = 500*									
		BSGM	BSGM _{fm}	BSGM _{cor}	UMA	MMA	BNMM	BSGM	BSGM _{fm}	BSGM _{cor}	UMA	MMA	BNMM	BSGM	BSGM _{fm}	BSGM _{cor}	UMA	BNMM			
A	Mean	NIE	8.67	8.44	8.61	0.02	-3.88	13.58	8.91	8.83	8.92	-0.02	7.58	8.91	8.83	8.92	-0.02	7.58			
		NDE	1.59	1.58	1.52	15.37	5.20	0.87	1.44	1.47	1.43	12.13	0.36	1.44	1.47	1.43	12.13	0.36			
		TE	10.26	10.02	10.14	15.39	1.32	14.45	10.35	10.35	10.30	10.35	12.11	7.95	10.35	10.30	10.35	12.11	7.95		
	Bias (%)	NIE	-6.21	-8.63	-6.77	-99.78	-141.99	46.97	-3.57	-4.49	-3.42	-100.22	-17.85	-3.57	-4.49	-3.42	-100.22	-17.85			
		NDE	13.64	13.02	8.77	997.86	271.42	-37.85	3.26	5.29	1.88	766.42	-74.26	3.26	5.29	1.88	766.42	-74.26			
		TE	-3.60	-6.13	-5.05	44.10	-86.54	35.30	-3.04	-3.48	-2.72	13.39	-25.52	-3.04	-3.48	-2.72	13.39	-25.52			
	Coverage (%)	NIE	90.40	83.60	88.00	1.60	3.20	47.60	90.80	89.20	92.40	0.40	48.80	90.80	89.20	92.40	0.40	48.80			
		NDE	92.80	88.80	90.40	0.80	3.60	42.80	96.00	93.60	95.60	1.20	39.20	96.00	93.60	95.60	1.20	39.20			
		TE	89.20	88.40	90.80	90.40	4.80	72.40	90.40	90.40	91.20	88.80	62.40	90.40	90.40	91.20	88.80	62.40			
	B	Sensitivity	NIE	0.90	0.90	0.90	0.00	0.12	0.15	0.90	0.90	0.90	0.07	0.24	0.90	0.90	0.90	0.07	0.24		
			NDE	1.00	0.99	0.98	0.97	0.99	0.91	1.00	0.99	1.00	0.98	0.84	1.00	0.99	1.00	0.98	0.84		
			TE	10.24	9.97	9.95	3.74	1.69	4.27	10.31	10.31	10.27	6.82	5.43	10.31	10.27	10.32	6.82	5.43		
Specificity		NIE	8.61	8.52	8.48	0.05	-2.72	3.36	8.90	8.84	8.89	0.03	3.71	8.90	8.84	8.89	0.03	3.71			
		NDE	1.63	1.45	1.47	3.69	4.41	0.91	1.41	1.43	1.43	6.79	1.72	1.41	1.43	1.43	6.79	1.72			
		TE	10.24	9.97	9.95	3.74	1.69	4.27	10.31	10.31	10.27	6.82	5.43	10.31	10.27	10.32	6.82	5.43			
Bias (%)		NIE	-6.78	-7.79	-8.22	-99.45	-129.44	-63.63	-3.71	-4.29	-3.78	-99.67	-59.86	-3.71	-4.29	-3.78	-99.67	-59.86			
		NDE	16.46	3.72	5.03	163.57	214.96	-35.01	1.03	2.05	2.33	385.06	22.82	1.03	2.05	2.33	385.06	22.82			
		TE	-3.72	-6.62	-6.48	-64.66	-84.18	-59.98	-3.45	-3.82	-3.33	-36.10	-49.17	-3.45	-3.82	-3.33	-36.10	-49.17			
Coverage (%)		NIE	89.20	84.00	86.40	0.80	0.00	36.80	91.20	89.60	93.20	0.00	40.80	91.20	89.60	93.20	0.00	40.80			
		NDE	90.00	90.00	90.80	16.40	1.20	58.80	93.60	90.40	94.00	5.20	62.40	93.60	90.40	94.00	5.20	62.40			
		TE	91.60	84.80	86.40	77.60	4.80	55.60	90.40	90.40	89.60	85.60	59.20	90.40	90.40	89.60	85.60	59.20			
Sensitivity	NIE	1.00	1.00	0.93	0.12	0.02	0.29	0.90	0.90	1.00	0.00	0.17	0.90	0.90	1.00	0.00	0.17				
	NDE	0.98	0.98	0.99	0.98	0.97	0.87	1.00	1.00	1.00	0.99	0.91	1.00	1.00	1.00	0.99	0.91				
	TE	10.10	9.83	10.10	17.55	1.17	17.09	10.42	10.34	10.34	11.60	8.07	10.42	10.34	10.38	11.60	8.07				
Mean	NIE	8.71	8.27	8.49	0.04	2.84	15.89	8.99	8.90	8.95	0.01	7.66	8.99	8.90	8.95	0.01	7.66				
	NDE	1.39	1.55	1.60	17.51	-1.67	1.20	1.43	1.44	1.43	11.59	0.41	1.43	1.44	1.43	11.59	0.41				
	TE	10.10	9.83	10.10	17.55	1.17	17.09	10.42	10.34	10.34	11.60	8.07	10.42	10.34	10.38	11.60	8.07				
Bias (%)	NIE	-5.79	-10.45	-8.11	-99.63	-69.26	71.45	-2.71	-3.70	-3.14	-99.89	-17.10	-2.71	-3.70	-3.14	-99.89	-17.10				
	NDE	-0.68	10.93	14.28	1150.71	-208.57	-14.29	2.15	3.02	2.11	727.86	-70.71	2.15	3.02	2.11	727.86	-70.71				
	TE	-0.68	10.93	14.28	1150.71	-208.57	-14.29	2.15	3.02	2.11	727.86	-70.71	2.15	3.02	2.11	727.86	-70.71				

TABLE 1 Continued

Residual Error	Scenario	N = 100										N = 500*									
		BSGM	BSGM _{fm}	BSGM _{cor}	UMA	MMA	BNMM	BSGM	BSGM _{fm}	BSGM _{cor}	UMA	MMA	BNMM	BSGM	BSGM _{fm}	BSGM _{cor}	UMA	MMA	BNMM		
A	TE	-5.11	-7.98	-5.52	64.33	-89.04	60.02	-2.49	-3.18	-3.13	8.61	-24.44									
	NIE	86.40	85.60	89.20	0.00	7.60	40.00	92.40	93.20	95.20	0.00	37.20									
	NDE	92.40	89.60	92.40	1.20	8.00	77.20	98.80	94.40	96.80	0.00	54.80									
	TE	90.40	86.40	88.80	83.60	13.60	54.40	94.40	93.60	93.20	96.80	30.40									
	Sensitivity	0.93	0.90	0.90	0.07	0.02	0.22	1.00	0.93	0.90	0.07	0.15									
	Specificity	1.00	0.98	0.99	0.97	0.98	0.90	1.00	1.00	1.00	0.99	0.86									
	Mean	8.68	8.49	8.63	0.01	-1.21	2.88	8.94	8.90	8.91	0.03	2.98									
	NDE	1.38	1.47	1.52	3.92	4.32	1.30	1.41	1.43	1.41	7.27	2.13									
	TE	10.06	9.96	10.15	3.93	3.11	4.18	10.35	10.34	10.32	7.30	5.11									
	NIE	-6.00	-8.11	-6.56	-99.89	-111.98	-68.74	-3.23	-3.63	-3.55	-99.67	-67.74									
B	NDE	-1.16	5.25	8.40	180.73	208.56	-7.14	0.82	2.47	0.90	52.14										
	TE	-5.36	-6.71	-4.59	-63.40	-70.88	-60.88	-2.69	-3.19	-3.33	-31.66										
	NIE	89.20	88.80	87.20	0.00	1.20	44.40	91.20	92.80	90.80	0.40	30.00									
	NDE	93.20	89.20	90.40	5.20	5.20	75.20	97.20	94.40	92.80	0.40	45.60									
	TE	90.00	90.00	86.00	78.40	6.00	58.00	92.00	93.20	91.60	92.80	38.40									
	Sensitivity	0.90	0.90	0.85	0.02	0.15	0.22	1.00	0.93	0.88	0.00	0.12									
	Specificity	1.00	0.97	0.98	0.98	0.91	0.84	0.99	0.96	0.99	0.99	0.94									

The evaluation metrics include mean or posterior mean (Mean), percentage bias (Bias), and frequentist coverage rate (Coverage) for estimating the natural indirect effect (NIE), natural direct effect (NDE), and total effect (TE), as well as the sensitivity and specificity for identifying mediating connections in the network.

*MMA is not included since it fails to converge under N = 500 within reasonable computational time (> 220h).

TABLE 2 Identified sub-networks from the mediation analyses and their overlaps with the functional system.

Functional system	Exposure		Outcome	Active	
	Subgraph 1	Subgraph 2	Subgraph	Subgraph 1	Subgraph 2
Default mode	10	14	7	5	4
Dorsal attention	2	2	0	0	0
Frontoparietal	3	5	0	0	0
Limbics	12	10	3	3	3
Somatomotor	10	11	4	4	4
Subcortical	12	12	2	1	2
Ventral attention	3	6	1	0	1
Visual	8	8	1	0	1
#of nodes	60	68	18	13	15
Weight mean	0.57	0.73	0.21	0.11	0.14

have both baseline MRI and diffusion tensor imaging (DTI) data collected in order to extract white matter fiber tracts to create structural connectivity. Among these participants, 26 experienced AD onset with the rest censored by death or loss of follow-up. In our analyses, we include gender, age at the screening visit, and years of education as covariates.

To construct structural connectivity for each subject, we first perform anatomical parcellation on the high-resolution T1-weighted anatomical MRI scan to obtain 68 gyral-based ROIs through the FreeSurfer. We employ the Lausanne parcellation scheme to subdivide these ROIs into 83 small ROIs. After preprocessing, including correction for motion and eddy current effects in DTI images, the DTI data are output to Diffusion Toolkit for fiber tracking. The FACT (fiber assignment by continuous tracking) algorithm is performed to initialize tracks from many seed points. It propagates these tracks along the most significant principal axis vector within each voxel until specific termination criteria are met. In this application, following previous structural connectivity studies (Zhao et al., 2023), we characterize each connection by the number of fiber tracks connecting the 2 ROIs divided by the mean volume of the corresponding ROI pairs. This induces a continuous measure for structural connection with each subject's structural connectivity summarized by an 83×83 connectivity matrix. As a demonstration, we randomly select a subject and show the fiber traits and the summarized connectivity matrix in Web Figure S3. For our genetic exposure APOE4+, we directly use the APOE genotyping data provided by the ADNI database. The data was generated for each participant at the time of enrollment using DNA extracted by Cogenics from a 3 mL aliquot of EDTA blood, and different APOE alleles were defined by SNPs rs429358 and rs7412. After summarizing the binary indicator for the presence of APOE ϵ 4 allele, the prevalence of APOE4+ is 0.48 across the cohort.

We perform mediation analysis using our proposed BSGM, which may be preferred over BSGM_{cor} given the sample size. The implementation details follow those in the simulations, and we visualize the normality of errors by residual Q-Q plots in Web Appendix D.2. Notably, a proportion of structural connections are 0 across all samples. To avoid model misspecification, we exclude these entries, along with the diagonal ones, following the procedure in model (1) for the connectivity matrix \mathbf{A}_i as well as random error vector \mathbf{e}_i . Eventually, we identify 2 subgraphs influ-

enced by the genotype and one impacting the outcome. The mediating subgraphs that bridge the genetic exposure to AD onset are obtained by overlapping these network components. Based on the posterior samples, we also estimate the NDE, NIE and TE with 95% credible intervals as $-1.36(-2.14, -0.68)$, $-0.04(-0.55, 0.43)$ and $-1.41(-2.44, -0.60)$, respectively. These results quantify the expected change on the log-survival time when altering genetic exposure, brain connectivity, and both. All 3 estimates are negative, indicating that APOE4+ will induce faster AD onset through both its direct effect and indirect effect mediated by brain structural connectivity. The 95% credible intervals for both the NDE and TE exclude 0. To further investigate how this effect mechanism functions along the identified brain subgraphs, we map the nodes in each subgraph to the canonical brain functional systems summarized in Table 2. As can be seen, the majority of the identified subgraphs involve the Default Mode, Limbic and Somatomotor systems. Relatedly, the existing literature reveals that Default Mode is one of the most well-known neuroimaging biomarkers for AD (Lee et al., 2016), and the Limbic system is also severely and routinely affected during neurodegeneration (Hopper and Vogel, 1976). We also provide visualizations for the identified subgraphs and the effect pathways they belong to in Figure 2, and illustrate the identified subgraphs are filled with cross-system connections. For the active mediating subgraphs, most of the cross-system connections are also among the Default Mode, Limbic, and Somatomotor systems. In contrast to the cross-system connections, there are only a small proportion of within-system connections as shown in Figure 2. This phenomenon is in accordance with the AD literature (Weiler et al., 2014), which suggests only sparse connections within functional systems in causing clinical symptoms and cognitive deficits. Finally, Figure 3 shows the components within the active mediating subgraphs that are negatively and positively linked with the disease onset outcome. While those sub-networks within individual subgraphs are not overlapping, there are common connections within and between canonical functional systems in both positive and negative sub-networks. Overall, both the characterization of the AD onset-related imaging genetics effect mechanism and the cartography of mediating brain network configurations provide important information to understand the etiology of the disease and direct future neuronal targets for genetic interventions.

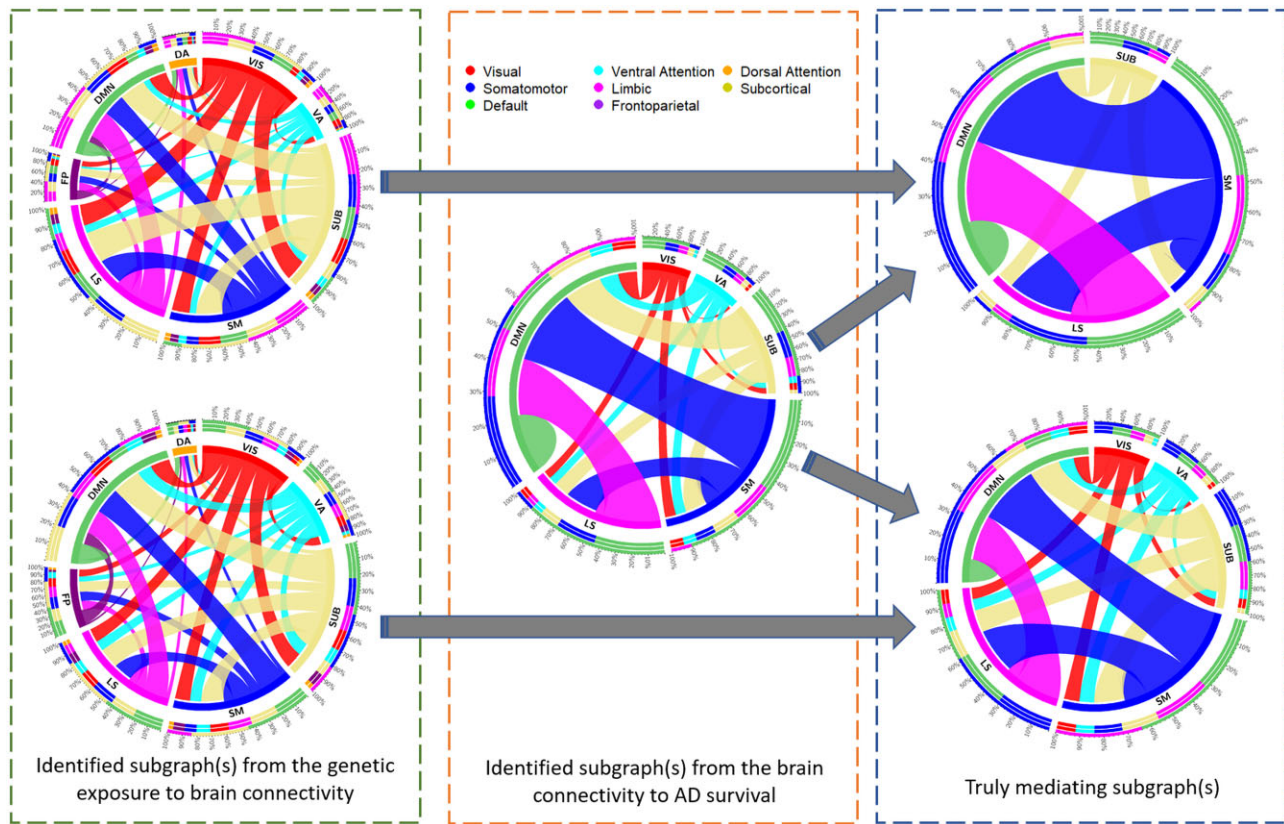


FIGURE 2 The brain network view for the identified subgraphs along each effect pathway as well as the potential mediating subgraphs.

6 DISCUSSION

In this paper, we propose a Bayesian mediation framework with a right-censored time-to-event outcome and a network-variate mediator to dissect the effect pathways among brain structural connectivity, genotype of interest, and time to disease onset. We develop a symmetric matrix-variate AFT model to characterize the effect pathway from brain connectivity to the outcome, and a symmetric matrix response regression to capture the impact from the genetic exposure to brain connectivity. By assuming structural connectivity operates along different effect paths through separate sets of clique subgraphs, we impose both within-graph sparsity and between-graph shrinkage to identify informative subgraph configurations and the active mediating network elements. We demonstrate the advantages of our method through extensive simulations and application to the landmark ADNI study.

In our modeling framework, we adopt the symmetric Tucker decomposition and assume that structural connectivity mediates the TE through distinct signaling subgraphs. An important direction for future work is to explore more robust nonparametric options to characterize the topological structure for connectivity. Additionally, because the connectivity matrix \mathbf{A}_i included nonnegative entries, a useful extension of our methodology is to allow for a link function in the mediator model. This would require a reformulation of the pathway effect measures in Proposition 1 and may increase the computational intensity

of our Bayesian algorithm. In our current application, we assign the same 0.5 prior probability for each node to be included in the signaling subgraphs (characterized by the selection indicators η_{hr} and γ_{jr}). Such a prior specification is noninformative and does not integrate potential scientific knowledge. Alternatively, should there be robust evidence from prior studies suggesting that certain brain regions are critical, one could assign a higher prior inclusion probability related to those brain regions to enhance the estimation efficiency and facilitate the interpretation of results. In [Web Appendix D.1](#), we provide comparisons with different informative priors based on a predetermined set of nodes under our ADNI application. Our findings confirm the robustness of the noninformative prior specification in estimating the direct and indirect effect, but demonstrate the sensitivity of the identified subgraphs to the choice of priors that leverage scientific knowledge. Finally, although our method currently focuses on a binary exposure, which is the most common setting in mediation analysis, it can be readily extended to accommodate a multi-category exposure. With a multi-category exposure, one can proceed by introducing dummy variables within the structural modeling framework (Hayes and Preacher, 2014), and update the identification expressions in Proposition 1. The proposed Bayesian inferential procedure should be straightforwardly adapted for pathway analysis with a multi-category exposure according to the updated mediation formulas.

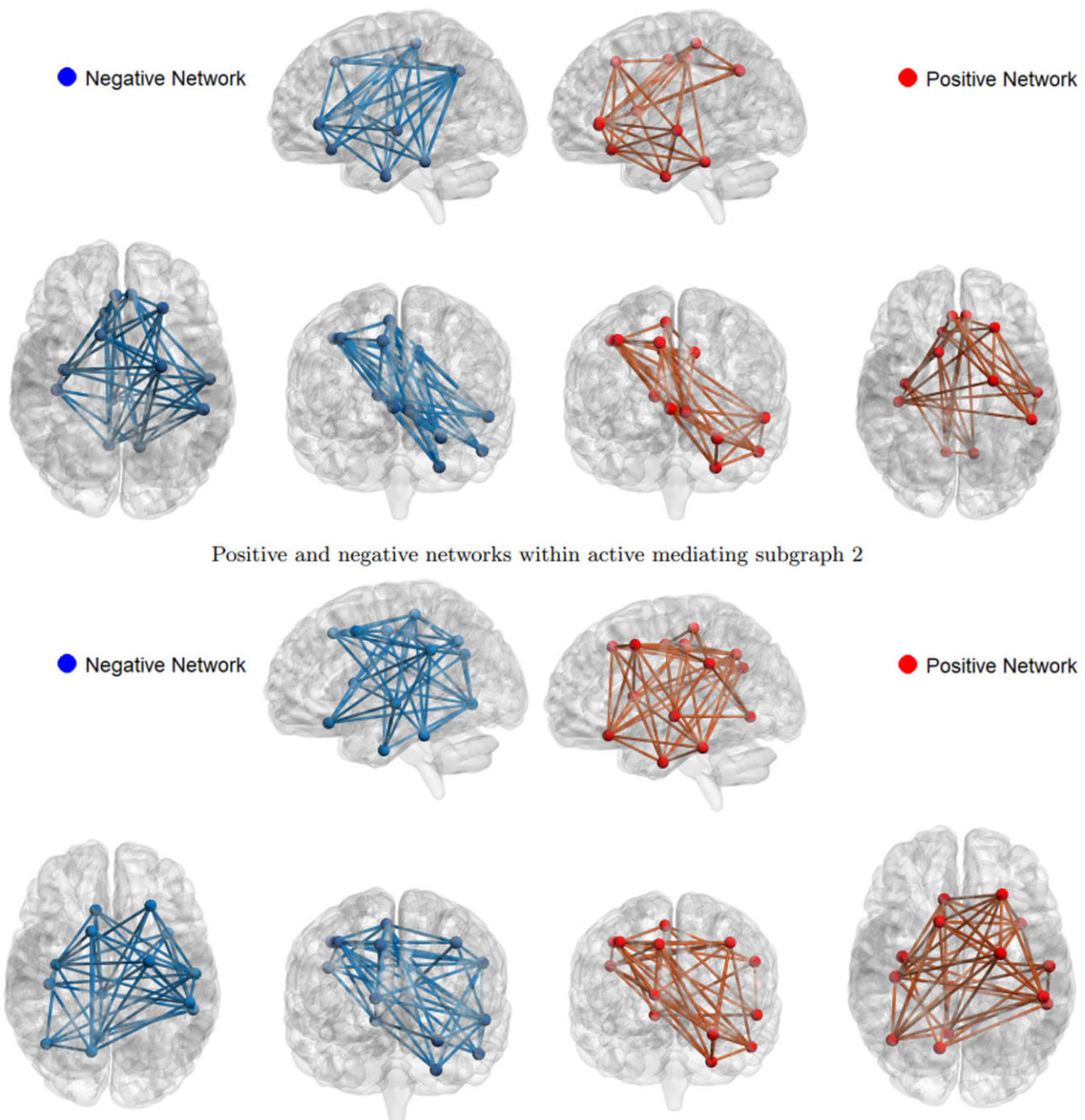


FIGURE 3 The identified sub-networks within the active mediating subgraphs that are negatively and positively linked with time to AD.

ACKNOWLEDGMENTS

The authors express their gratitude to the associate editor and 2 referees for their constructive and insightful comments and suggestions, which have greatly improved the quality of the paper.

SUPPLEMENTARY MATERIALS

Supplementary material is available at *Biometrics* online.

Web Appendices, Tables, Figures, referenced in Sections 2–6, and sample code for implementation are available with this paper at the *Biometrics* website on Oxford Academic.

FUNDING

This work was partially funded by RF1AG081413, R01EB034720, R01AG068191, P30AG066508, and UL1TR001863 from the National Institutes of Health (NIH).

CONFLICT OF INTEREST

None declared.

DATA AVAILABILITY

The data that support the findings in this paper are openly available in the Alzheimer's Disease Neuroimaging Initiative (ADNI) database at <http://adni.loni.usc.edu>.

REFERENCES

- Ballester-Plané, J., Schmidt, R., Laporta-Hoyos, O., Junqué, C., Vázquez, É., Delgado, I. et al. (2017). Whole-brain structural connectivity in dyskinetic cerebral palsy and its association with motor and cognitive function. *Human Brain Mapping*, 38, 4594–4612.
- Barbieri, M. M. and Berger, J. O. (2004). Optimal predictive model selection. *The Annals of Statistics*, 32, 870–897.
- Bassett, D. S. and Sporns, O. (2017). Network neuroscience. *Nature Neuroscience*, 20, 353–364.
- Chén, O. Y., Crainiceanu, C., Ogburn, E. L., Caffo, B. S., Wager, T. D. and Lindquist, M. A. (2018). High-dimensional multivariate mediation with application to neuroimaging data. *Biostatistics*, 19, 121–136.
- Chen, T., Mandal, A., Zhu, H. and Liu, R. (2022). Imaging genetic based mediation analysis for human cognition. *Frontiers in Neuroscience*, 16, 824069.
- Derkach, A., Pfeiffer, R. M., Chen, T.-H. and Sampson, J. N. (2019). High dimensional mediation analysis with latent variables. *Biometrics*, 75, 745–756.
- Gelman, A. and Rubin, D. B. (1992). Inference from iterative simulation using multiple sequences. *Statistical Science*, 7, 457–472.
- Guhaniyogi, R., Qamar, S. and Dunson, D. B. (2017). Bayesian tensor regression. *Journal of Machine Learning Research*, 18, 1–31.
- Hashimoto, R., Ohi, K., Yamamori, H., Yasuda, Y., Fujimoto, M., Umeda-Yano, S. et al. (2015). Imaging genetics and psychiatric disorders. *Current Molecular Medicine*, 15, 168–175.
- Hayes, A. F. and Preacher, K. J. (2014). Statistical mediation analysis with a multicategorical independent variable. *British Journal of Mathematical and Statistical Psychology*, 67, 451–470.
- Hopper, M. and Vogel, F. (1976). The limbic system in Alzheimer's disease. a neuropathologic investigation. *The American Journal of Pathology*, 85, 1–20.
- Huang, Y. T. and Yang, H. I. (2017). Causal mediation analysis of survival outcome with multiple mediators. *Epidemiology*, 28, 370–378.
- Imai, K., Keele, L. and Tingley, D. (2010). A general approach to causal mediation analysis. *Psychological Methods*, 15, 309.
- Imai, K. and Yamamoto, T. (2013). Identification and sensitivity analysis for multiple causal mechanisms: Revisiting evidence from framing experiments. *Political Analysis*, 21, 141–171.
- Kolda, T. G. and Bader, B. W. (2009). Tensor decompositions and applications. *SIAM Review*, 51, 455–500.
- Lee, E., Yoo, K., Lee, Y., Chung, J., Lim, J., Yoon, B. and Jeong, Y. (2016). Default mode network functional connectivity in early and late mild cognitive impairment: Results from the Alzheimer's disease neuroimaging initiative. *Alzheimer Disease & Associated Disorders*, 30, 289–296.
- Lindquist, M. A. (2012). Functional causal mediation analysis with an application to brain connectivity. *Journal of the American Statistical Association*, 107, 1297–1309.
- Park, T. and Casella, G. (2008). The Bayesian lasso. *Journal of the American Statistical Association*, 103, 681–686.
- Schoot, R., Kaplan, D., Denissen, J., Asendorpf, J., Neyer, F. and Aken, M. (2013). A gentle introduction to Bayesian analysis: Applications to developmental research. *Child Development*, 85, 842–860.
- Song, Y., Zhou, X., Zhang, M., Zhao, W., Liu, Y., Kardia, S. L. et al. (2020). Bayesian shrinkage estimation of high dimensional causal mediation effects in omics studies. *Biometrics*, 76, 700–710.
- Sun, W., Chang, C., Zhao, Y. and Long, Q. (2018). Knowledge-guided Bayesian support vector machine for high-dimensional data with application to analysis of genomics data. In: *2018 IEEE International Conference on Big Data (Big Data)*, 1484–1493. IEEE.
- Tian, X., Wang, Y., Wang, S., Zhao, Y. and Zhao, Y. (2024). Bayesian mixed model inference for genetic association under related samples with brain network phenotype. *Biostatistics*, 25, 1195–1209.
- VanderWeele, T. J. (2011). Causal mediation analysis with survival data. *Epidemiology*, 22, 582.
- Wang, L., Lin, F. V., Cole, M. and Zhang, Z. (2021). Learning clique subgraphs in structural brain network classification with application to crystallized cognition. *NeuroImage*, 225, 117493.
- Wang, W., Nelson, S. and Albert, J. M. (2013). Estimation of causal mediation effects for a dichotomous outcome in multiple-mediator models using the mediation formula. *Statistics in Medicine*, 32, 4211–4228.
- Weiler, M., Campos, B., Nogueira, M., Damasceno, B., Cendes, F. and Balthazar, M. (2014). Structural connectivity of the default mode network and cognition in Alzheimer's disease. *Psychiatry Research: Neuroimaging*, 223, 15–22.
- Zhao, Y., Chang, C., Zhang, J. and Zhang, Z. (2023). Genetic underpinnings of brain structural connectome for young adults. *Journal of the American Statistical Association*, 118, 1473–1487.
- Zhao, Y., Chen, T., Cai, J., Lichenstein, S., Potenza, M. and Yip, S. (2022). Bayesian network mediation analysis with application to brain functional connectome. *Statistics in Medicine*, 41, 3991–4005.
- Zhao, Y., Li, L. and Caffo, B. S. (2021). Multimodal neuroimaging data integration and pathway analysis. *Biometrics*, 77, 879–889.
- Zhao, Y. and Luo, X. (2019). Granger mediation analysis of multiple time series with an application to functional magnetic resonance imaging. *Biometrics*, 75, 788–798.
- Zhu, H., Khondker, Z., Lu, Z. and Ibrahim, J. G. (2014). Bayesian generalized low rank regression models for neuroimaging phenotypes and genetic markers. *Journal of the American Statistical Association*, 109, 977–990.